ROBUSTNESS OF LAPLACE DOMAIN WAVEFORM INVERSIONS TO CYCLE SKIPPING

DONGHYUN RYU[1], AHREUM KIM[1], WANSOO HA[1] and CHANGSOO SHIN[2]

1 Department of Energy Resources Engineering, Pukyong National University, Busan, South Korea.
wansooha@pknu.ac.kr
2 Department of Energy Resources Engineering, Seoul National University, Seoul, South Korea.

(Received May 17, 2016; revised version accepted March 11, 2017)

ABSTRACT

Ryu, D., Kim, A., Ha, W. and Shin, C., 2017. Robustness of Laplace domain waveform inversions to cycle skipping. *Journal of Seismic Exploration*, 26: 251-266.

The local minima problem introduced by cycle skipping is an important barrier for a successful waveform inversion. However, numerical examples of the Laplace-domain full waveform inversions show that we can start from simple initial models to obtain subsurface models, without the local minima problem. Although we can infer that the Laplace-domain inversion is robust to the cycle skipping problem from previous literatures, theoretical examination about the effect of cycle skipping in the Laplace domain is missing. We explain why the Laplace-domain logarithmic objective function is robust to cycle skipping by examining the effect of time shifts of seismic traces on the objective function. A test using a sine wavelet shows that the Laplace transform converts the time shift in the time domain to an amplitude change in the Laplace domain. The amplitude change due to the time shift shows monotonous variations as the amount of time shift increases. Therefore, no cycle skipping effect in the Laplace domain is evident, and the Laplace domain objective function shows a monotonous variation. Numerical examples using 1D and 2D models demonstrate that the Laplace domain objective function is robust to cycle skipping.

KEY WORDS: Laplace domain, full waveform inversion, cycle skipping.

INTRODUCTION

Correct subsurface model information is crucial for successful subsurface imaging. There are several kinds of techniques to obtain subsurface model parameters, such as travel time tomography (White, 1989), stereotomography (Billette and Lambaré, 1998), migration velocity analysis (Liu and Bleistein, 1995), and full waveform inversion (Tarantola, 1984). Full waveform inversion is one of the most advanced techniques for subsurface estimation. It updates the

0963-0651/17/$5.00

subsurface model to the direction that minimizes the differences between the observed and modeled seismic data (Tarantola, 1984).

There are two kinds of optimization strategies for full waveform inversions. Global optimization methods try to find the global minimum or maximum using appropriate constraints (Landa et al., 1989; Sen and Stoffa, 1991; Stoffa and Sen, 1991). On the other hand, local-gradient-based optimization methods use the gradient direction of the objective function at the current position to find a neighboring minimum or maximum. Most waveform inversion methods use a form of the local-gradient-based optimization approach due to the computational burden. The local minimum is a critical barrier for successful convergence in this approach. Major sources of the local minima include the cycle skipping of the seismic signal, noises, and simplified governing equations for wave propagation. An accurate starting model or a robust objective function is required to avoid the local minima problem (Virieux and Operto, 2009).

Time- or frequency-domain full waveform inversions combined with travel time tomography (Brenders and Pratt, 2007) or stereotomography (Prieux et al., 2012) attempt to obtain a better starting model to avoid the local minima. Multiscale or sequential approaches avoid the local minima by starting inversion from low-frequency data, which contains fewer local minima in their objective functions (Bunks et al., 1995; Sirgue and Pratt, 2004; Ravaut et al., 2004). These methods use the results of lower frequency inversions as the starting models for higher frequency inversions to approach the global minimum. Research has been conducted to find more robust objective functions (Guitton and Symes, 2003; Ha et al., 2009; Brossier et al., 2010; Alkhalifah and Choi, 2012; Warner and Guasch, 2014; Wu et al., 2014).

Laplace-domain full waveform inversions, unlike the time- or frequency-domain inversions, successfully yield inversion results with poor starting models. The inversion can start from constant velocity models or simple gradient models (Ha et al., 2012; Ha and Shin, 2012; Pyun et al., 2010; Shin et al., 2013; Shin and Cha, 2008; Shin and Ha, 2008; Shin et al., 2014), which implies that the Laplace domain objective function is not sensitive to the cycle skipping problem. However, theoretical examination of the cycle skipping in the Laplace domain is not presented yet.

In this study, we explain why the Laplace-domain logarithmic objective function is robust to the cycle skipping problem. We first examine the effect of the time shift of a simple time-domain signal on the logarithmic objective function in the Laplace domain. We compare the time- and frequency-domain L_2 objective function with the Laplace-domain objective function. Then, we use 1D and 2D examples with one variable to depict the behavior of the objective function.

EFFECT OF CYCLE SKIPPING ON OBJECTIVE FUNCTIONS IN TIME, FREQUENCY AND LAPLACE DOMAINS

We examine the effect of cycle skipping on the objective functions in time, frequency, and Laplace domains. We chose common objective functions for each domain. The time domain L_2 objective function (Tarantola, 1984; Mora, 1987) is defined as:

$$E(t) = \tfrac{1}{2} \int_0^\infty [p(t) - d(t)]^2 dt \quad , \tag{1}$$

where p(t) is the modeled wavefield, and d(t) is the observed wavefield. When there are multiple receivers and sources, we can use the summation over receivers and sources. The frequency domain L_2 objective function (Pratt et al., 1998; Pratt, 1999) is

$$E(\omega) = \tfrac{1}{2}[\tilde{p}(\omega) - \tilde{d}(\omega)][\tilde{p}(\omega) - \tilde{d}(\omega)]^* \quad , \tag{2}$$

where * indicates the complex conjugate, α is the angular frequency, and

$$\begin{aligned} \tilde{p}(\omega) &= \int_{-\infty}^{\infty} p(t) e^{-i\omega t} dt \quad , \\ \tilde{d}(\omega) &= \int_{-\infty}^{\infty} d(t) e^{-i\omega t} dt \quad . \end{aligned} \tag{3}$$

The Laplace domain logarithmic objective function (Shin and Cha, 2008) is

$$E(s) = \tfrac{1}{2}\{\ln[\hat{p}(s)/\hat{d}(s)]\}^2 \quad , \tag{4}$$

where s is a positive damping constant, and

$$\begin{aligned} \hat{p}(s) &= \int_0^\infty p(t) e^{-st} dt \quad , \\ \hat{d}(s) &= \int_0^\infty d(t) e^{-st} dt \quad . \end{aligned} \tag{5}$$

Note that the frequency- and Laplace-domain objective functions are calculated using single frequency or damping constant while the time-domain objective function is integrated over time.

We generated a 0.5 Hz sine signal that was padded with zeros for the examination. The synthetic signal is defined as:

$$d(t) = \begin{cases} 0 & , \ 0 \leq t \leq 2 \\ \sin(\pi t) & , \ 2 \leq t \leq 8 \\ 0 & , \ 8 \leq t \leq 10 \end{cases} , \tag{6}$$

where the first arrival time is 2 s. We set this signal as the observed wavefield and generated the modeled wavefield by applying time-shift, τ, to the signal to mimic cycle skipping. We used a zero-padded simple signal and time shift to isolate the effect of cycle skipping from the effect of amplitude change. We defined the modeled wavefield as:

$$p(t) = d(t - \tau) \ , \tag{7}$$

where $-2 \leq \tau \leq 2$. We limited the time shift from -2 s to 2 s to avoid changes in the shape of the sine wavelet. Fig. 1 shows the observed and the two modeled wavelets with different time shift. Note that there is no cycle skipping between the top and middle wavelets; however, we can see cycle skipping between the top and bottom wavelets. Because we used a 0.5 Hz sine wavelet, cycle skipping occurs when the absolute value of the time shift is larger than 1s, which is equivalent to half of the period of the signal (Virieux and Operto, 2009).

We can see the effect of cycle skipping on the time- and frequency-domain objective functions in Figs. 2a and 2b. When the absolute value of the time shift is larger than 1 s, cycle skipping occurs, and the objective functions in the time and frequency domains are directed towards the local minima. The time shift changes the phase of the frequency-domain wavefield, which can suffer from phase wrapping (Alkhalifah and Choi, 2012).

On the other hand, the Laplace-domain logarithmic objective function behaves differently when there is a time shift. We can obtain the modeled Laplace domain wavefield by Laplace transforming the time-shifted signal as:

$$\hat{p}(s) = \int_0^\infty p(t)e^{-st}dt = \int_0^\infty d(t - \tau)e^{-st}dt \ . \tag{8}$$

By substituting $x = t - \tau$ in the equation above, we can derive the following equation:

$$\hat{p}(s) = \int_{-\tau}^{\infty} d(x)e^{-s(x+\tau)}dx$$

$$= e^{-s\tau} \int_{-\tau}^{\infty} d(x)e^{-sx}dx$$

$$= e^{-s\tau}[\int_{-\tau}^{0} d(x)e^{-sx}dx + \int_{0}^{\infty} d(x)e^{-sx}dx]$$

$$= e^{-s\tau}[\int_{-\tau}^{0} d(x)e^{-sx}dx + \hat{d}(s)]$$

$$= \hat{d}(s)e^{-s\tau} \quad . \tag{9}$$

The term $\int_{-\tau}^{0} d(x)e^{-sx}$ equals 0 when the time shift is larger than 0 because the signal is causal. When the time shift is smaller than 0, the term $\int_{-\tau}^{0} d(x)e^{-sx}$ still equals 0 because $-\tau$ is not larger than the first arrival time.

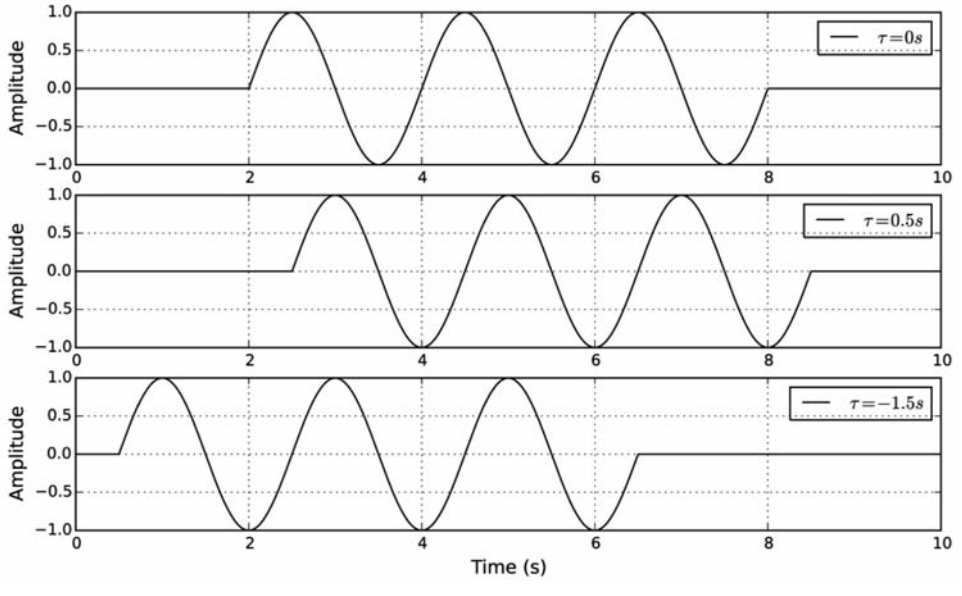

Fig. 1. A synthetic signal used for the analysis. The signals in the middle and bottom panels are time-shifted version of the original signal in the top panel.

Note that the time-shifted signal differs from the original signal by the term $e^{-s\tau}$. The time shift changes the amplitude of the Laplace-domain wavefield. As the time shift increases, the amplitude decreases monotonously. The amplitude also increases monotonously as the time shift decreases. Therefore, the Laplace-domain objective function always increases whether the time shift increases or decreases.

We can substitute eq. (9) in eq. (4) to calculate the objective function as

$$E(s) = \tfrac{1}{2}\{\ln[\hat{p}(s)/\hat{d}(s)]\}^2 = \tfrac{1}{2}\{\ln[\hat{d}(s)e^{-s\tau}/\hat{d}(s)]\}^2 = \tfrac{1}{2}\{\ln(e^{-s\tau})\}^2$$

$$= \tfrac{1}{2}(-s\tau)^2 = (s\tau)^2/2 \quad . \tag{10}$$

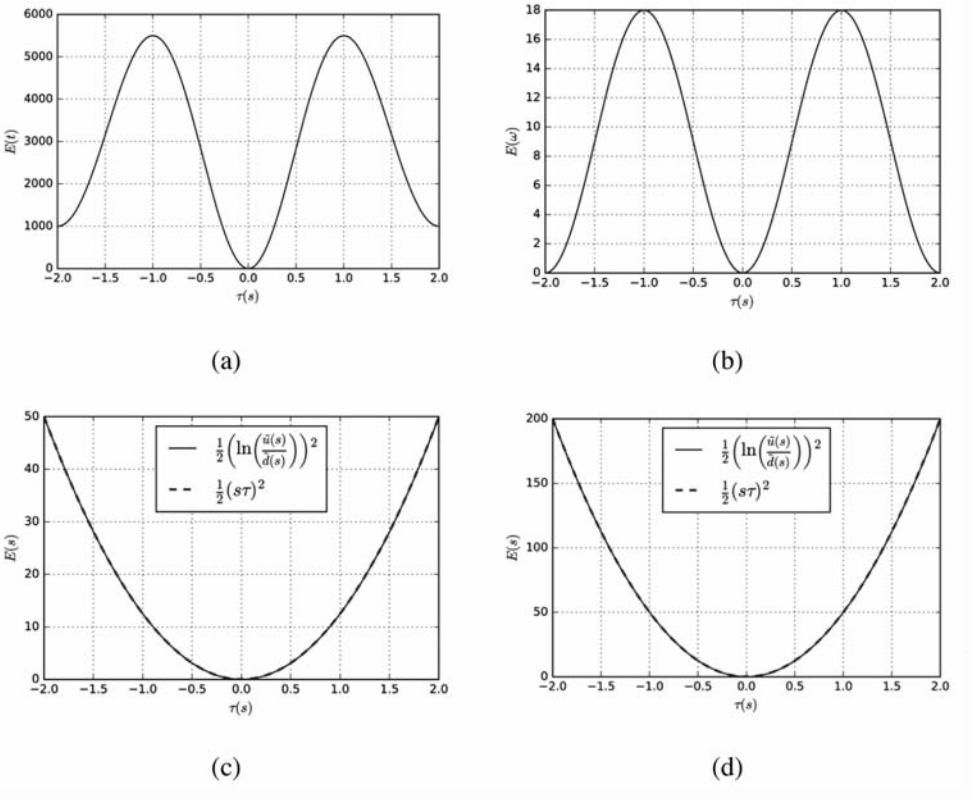

Fig. 2. Objective functions calculated using the time-shifted signals. (a) the time-domain L_2 objective function, (b) the frequency-domain L_2 objective function when the frequency is 0.5 Hz, and the Laplace-domain logarithmic objective functions when the damping constant is (c) 5 s^{-1}, and (d) 10 s^{-1}, respectively.

The result is a quadratic function of τ. There is no local minimum in the function above, regardless of cycle skipping. Figs. 2c and 2d show that the Laplace-domain objective functions calculated using eq. (4) and eq. (10) match exactly.

NUMERICAL EXAMPLES

We simulated seismic wavefields using 1D and 2D models. The 1D model contains 3 layers (Fig. 3a). The velocities of each layer are 1.5, 2.5, and 3.5 km/s. We generated the observed seismic signal using the acoustic wave equation and a Ricker source wavelet (Fig. 3b). Fig. 4a shows the seismogram. We extracted the trace at the surface from the seismogram and calculated the objective functions with the modeled data obtained by varying the velocity of the second layer. The velocity of the second layer varies from 1.0 to 4.0 km/s at the interval of 0.1 km/s. Fig. 4b shows the observed data and the modeled data with different velocities. The wavelet at 1.5 s is the reflected wave from the interface between the first and second layers. As the velocity of the second layer varies, the amplitude of the first reflected wave changes. The wavelet at 2.3 s is the reflected wave from the interface between the second and third layers. The velocity change introduces both amplitude change and time shift to the second reflected wave. The main source of cycle skipping in this example is the time shift of the second reflected wave.

Fig. 5 shows the objective functions obtained in the time, frequency, and Laplace domains. The time-domain objective function (Fig. 5a) shows a very narrow convex area. There are local minima close to the true velocity because a small variation of the velocity introduces cycle skipping of the second reflection event. Unless we start from an accurate initial model, finding the true velocity model using a local-gradient based optimization method is difficult. Frequency-domain objective functions at 3 and 6 Hz (Figs. 5b and 5c) also contain local minima. The convex area is broader at lower frequencies, as demonstrated by many researchers (Bunks et al., 1995; Shin and Ha, 2008; Shin and Cha, 2008). On the other hand, Laplace-domain objective functions show no local minima, regardless of the damping constant (Figs. 5d and 5e).

We also tested a 2D velocity model. Fig. 6a shows the AA' profile of the SEG/EAGE 3D salt model (Aminzadeh et al., 1994). We generated additional velocity models to obtain the modeled data by varying the velocity of the salt body from 2.0 to 6.0 km/s at the interval of 0.1 km/s. The true velocity of the salt body used to obtain the observed data is 4.45 km/s. We modeled the acoustic wave propagation for 10 s with one source at the center of the surface. Figs. 6b and 6c show the modeled and observed shot obtained from the velocity models with the velocity of the salt of 3.5 and 4.45 km/s, respectively. We extracted traces at 12 km from the left for comparison (Fig. 7a). We can

observe cycle skipping between the observed and modeled traces. However, the Laplace-domain wavefields obtained from different salt velocities show only mild amplitude variations (Fig. 7b). The amplitude change and time shift in the time-domain wavefields are merged into the amplitude change in the Laplace domain. The variation of the amplitude is larger at a longer offset for a fixed damping constant because the move-out is larger at the longer offset. Unlike the time-domain objective function, Laplace-domain objective functions contain no local minimum (Fig. 8). Frequency-domain objective functions show similar behaviors to those in the previous 1D example (Shin and Ha, 2008; Shin and Cha, 2008).

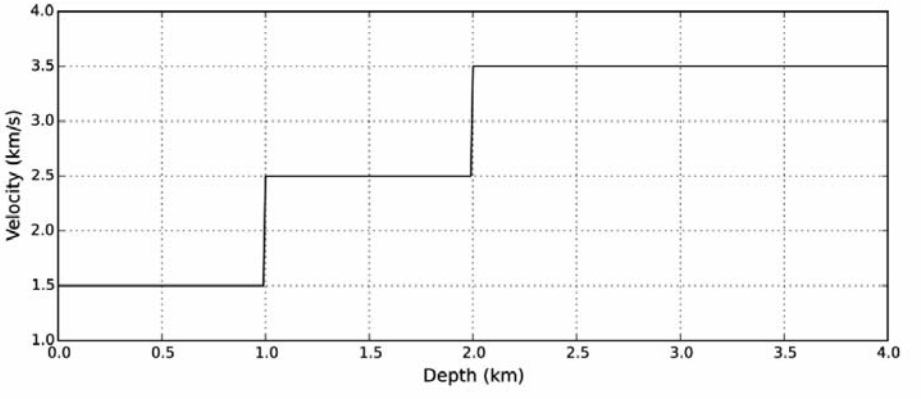

(a)

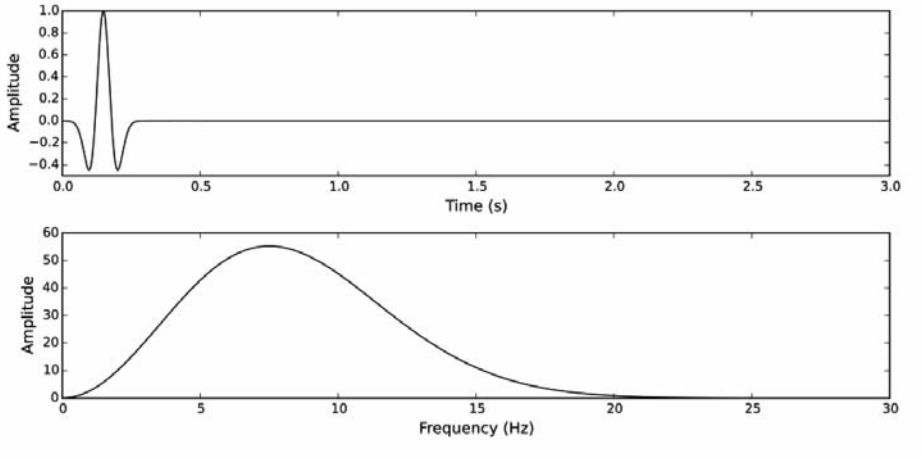

(b)

Fig. 3. (a) A 3-layer 1D velocity model, and (b) the source wavelet used in the example and its amplitude spectrum.

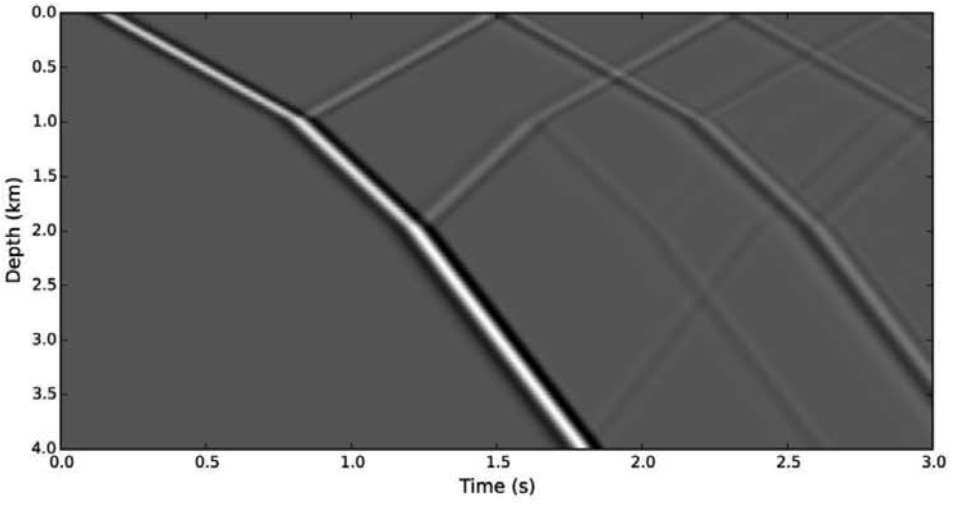

(a)

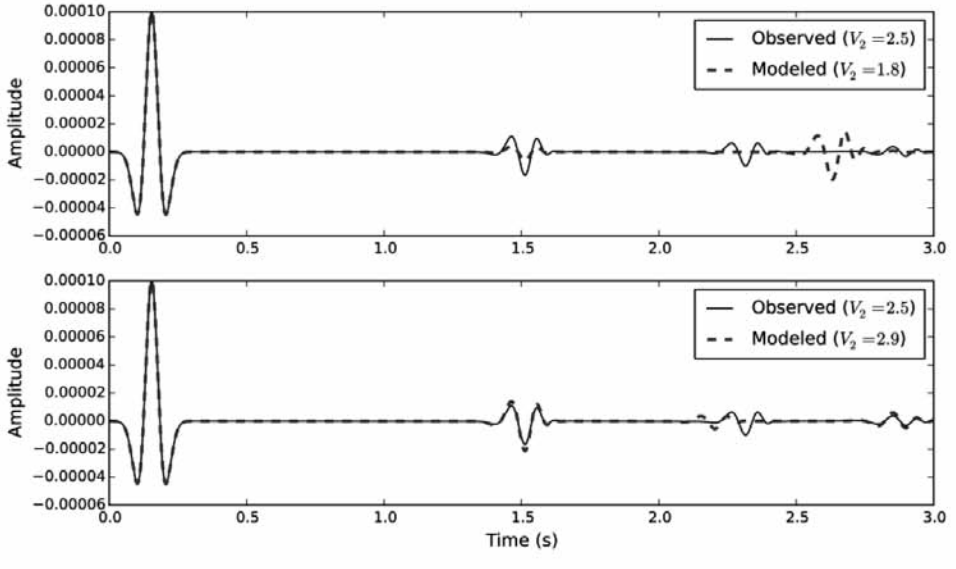

(b)

Fig. 4. (a) The recorded seismogram, and (b) the surface seismograms from different second-layer velocities.

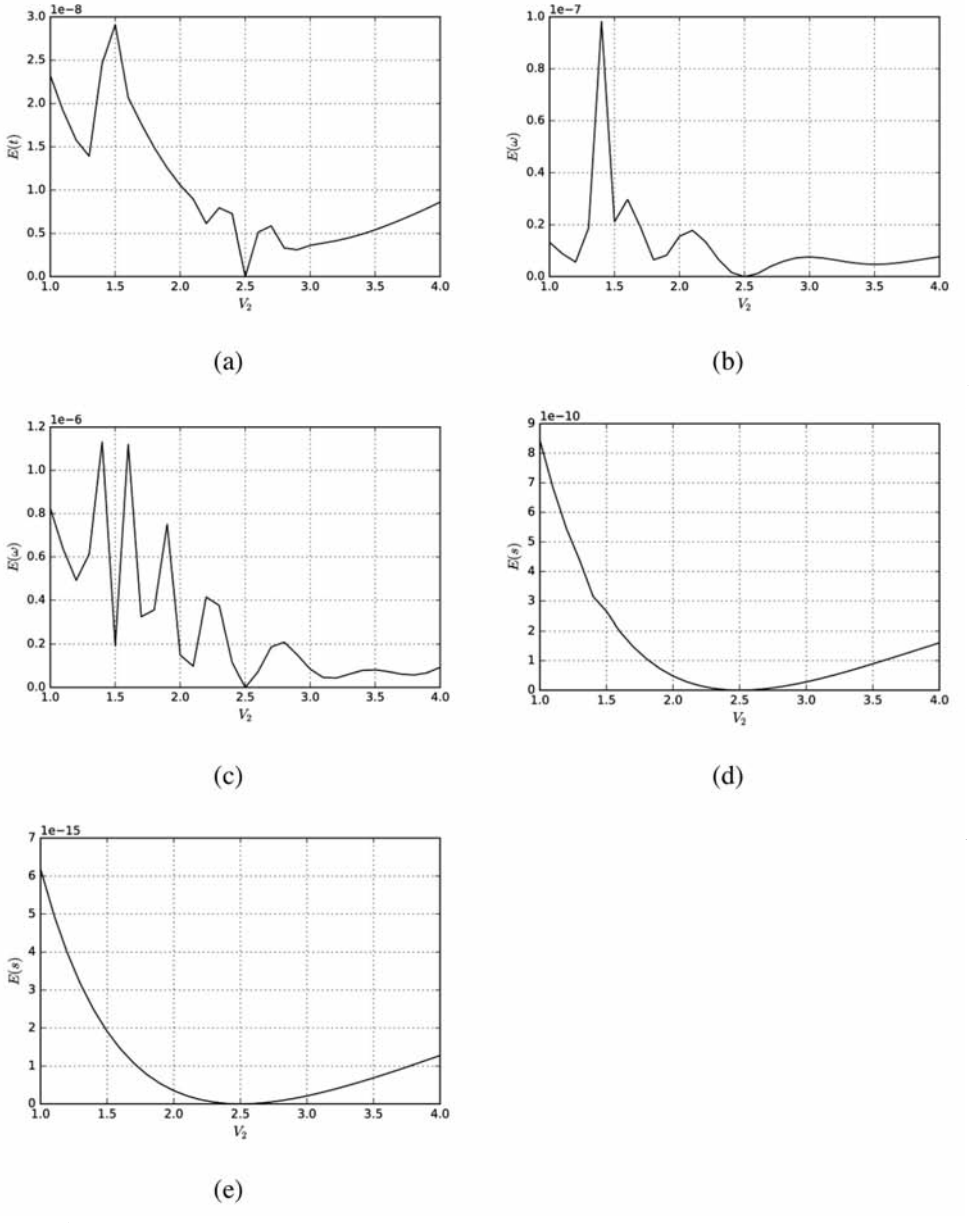

Fig. 5. Objective functions as functions of the velocity of the 2nd layer. (a) The time-domain L_2 objective function, and the frequency-domain L_2 objective functions when the frequency is (b) 3 Hz, and (c) 6 Hz. The Laplace-domain logarithmic objective functions when the damping constant is (d) 5 s^{-1}, and (e) 10 s^{-1}, respectively.

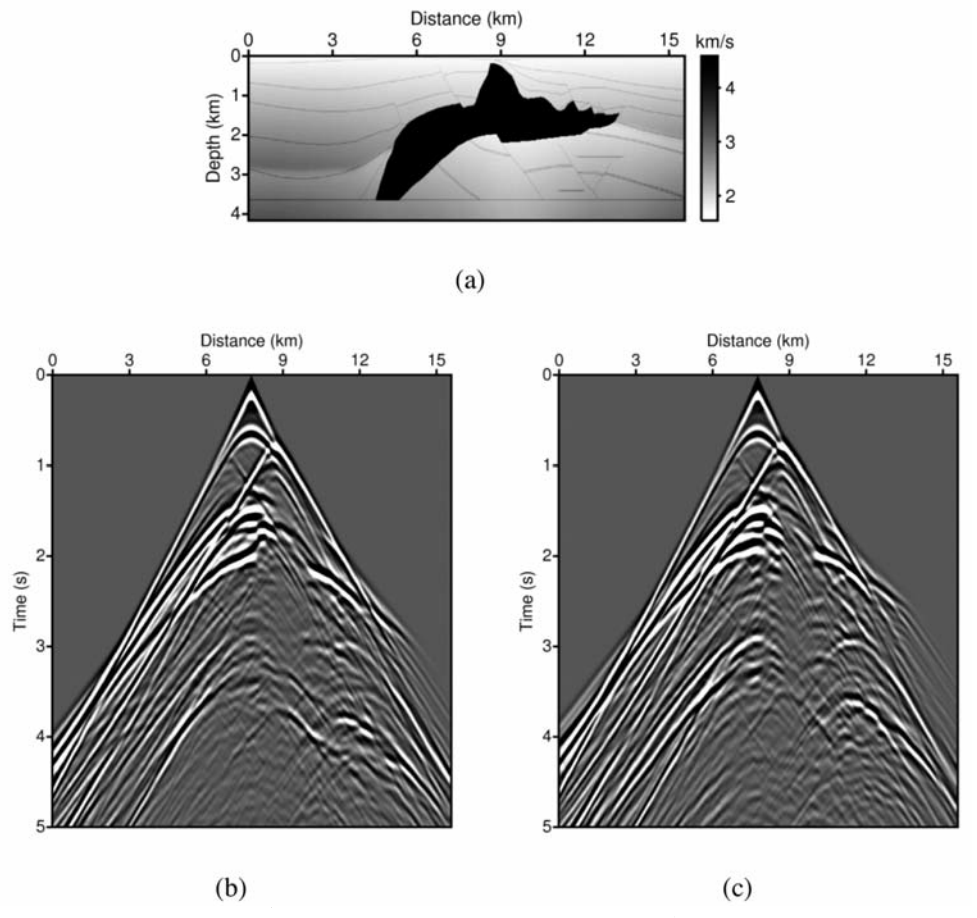

Fig. 6. (a) The AA′ profile of the SEG/EAGE 3D salt model (Aminzadeh et al., 1994). Shot gathers shown up to 5 s obtained using the velocity of salt as (b) 3.5 km/s and (c) 4.45 km/s.

DISCUSSION

We could observe no local minimum in the previous examples with one variable; however, Laplace-domain objective functions also have local minima with lots of model parameters and noise. However, they have a larger convex area than those of time- or frequency-domain L_2 objective functions. There are many examples in the literature demonstrating the ability of the Laplace-domain inversion to start from a scratch model and converge (Ha et al., 2012; Ha and Shin, 2012; Pyun et al., 2010; Shin et al., 2013, 2014).

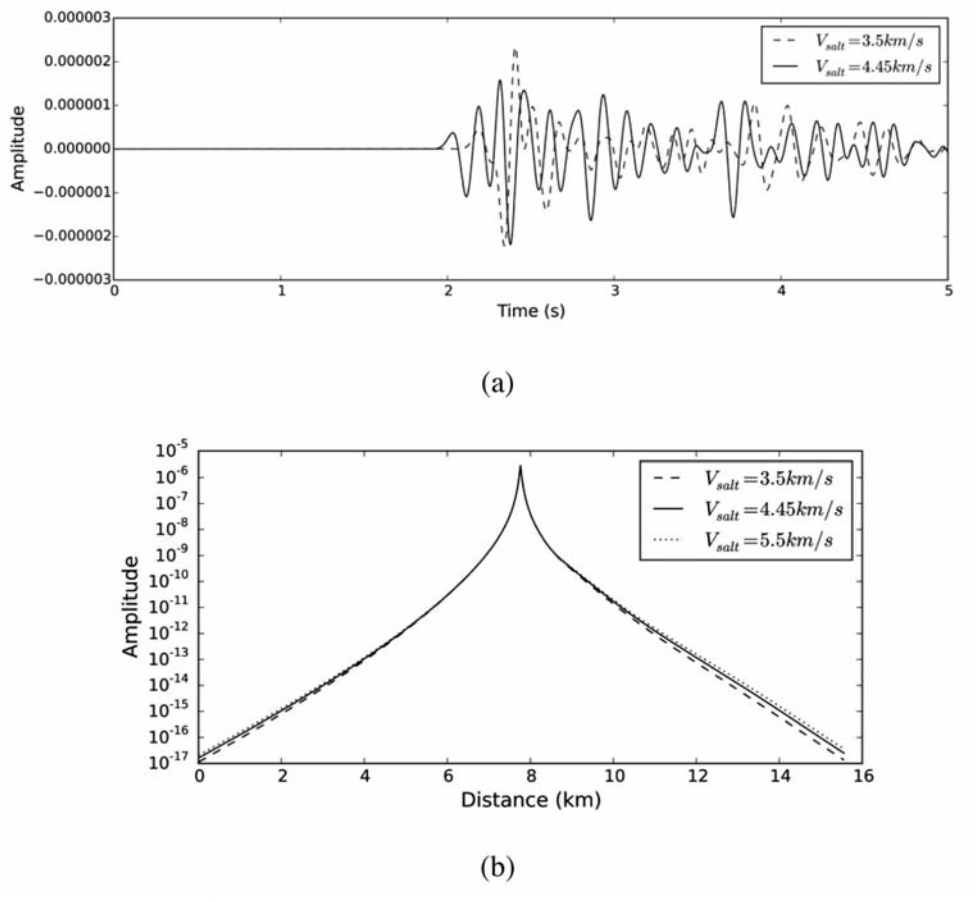

Fig. 7. (a) Traces at 12 km from the left in Fig. 6b and c. (b) Laplace transform of the shot gathers in Fig. 6b and c when the damping constant is 5 s^{-1}.

One important source of the local minimum in the Laplace domain is the maximum recording time. Because Laplace-transform of the observed data involves the Laplace transform [eq. (5)], we need long recording times for a stable transform, particularly when the damping constant is low (Ha et al., 2012). Fig. 9 shows the Laplace-domain objective function of the 2D salt example with the damping constant of 5 s^{-1}, when the maximum recording time is 4 s. We can observe local minima in the objective function. The stability problem is more severe when the damping constant is low. We can use a high damping constant without a stability problem; however, we need to invert a low damping constant to obtain information from the depth (Ha et al., 2012).

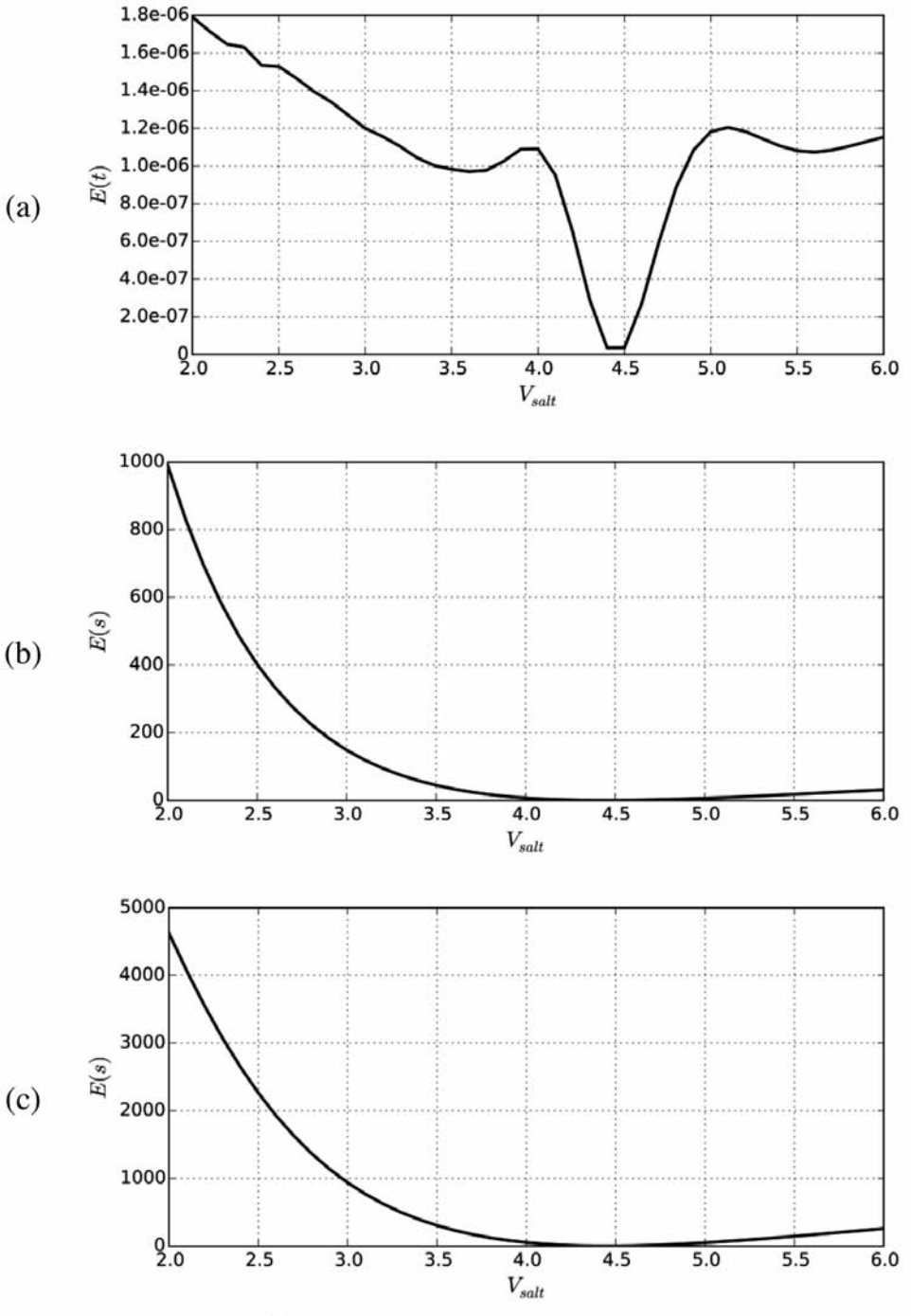

Fig. 8. Objective functions as functions of the velocity of the salt. (a) The time-domain L_2 objective function, and the Laplace-domain logarithmic objective functions when the damping constant is (b) 5 s^{-1}, and (c) 10 s^{-1}, respectively.

Therefore, seismic data with a long recording time is required for a stable convergence of the Laplace-domain full waveform inversion. When data with a long recording time is not available, simultaneous inversions of both low and high damping constants (Shin and Cha, 2008) or sequential inversion approaches starting from high damping can mitigate the local minima problem in the Laplace domain (Shin et al., 2010).

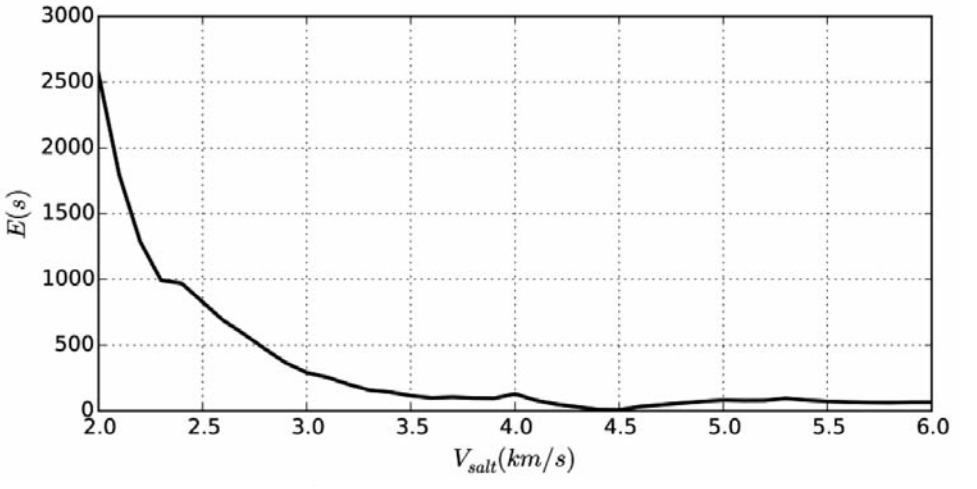

Fig. 9. The Laplace domain objective function with the maximum recording time of 4 s and the damping constant of 5 s^{-1}.

CONCLUSIONS

We demonstrated why the logarithmic objective function of the Laplace domain inversion is robust to cycle skipping. Cycle skipping occurs because of the time shift of a seismic wavelet from inaccurate subsurface parameters. Time- or frequency-domain objective functions show cyclic behavior as the time shift increases and develop local minima. On the other hand, the Laplace-domain logarithmic objective function does not have the local minima problem introduced by cycle skipping. The increased time shift changes the amplitude of the Laplace-domain wavefields monotonously, which explains why Laplace-domain inversions are robust to poor initial models. Dependency on the recording time is a limitation of the Laplace-domain inversion methods, and we need further studies to stabilize the Laplace-domain inversion of data with a short recording time and low damping constants.

ACKNOWLEDGMENTS

This research was supported by the Basic Research Project (15-3313) of the Korea Institute of Geoscience and Mineral Resources (KIGAM) funded by the Ministry of Science, ICT and Future Planning of Korea, and the Supercomputing Center/Korea Institute of Science and Technology Information with supercomputing resources (KSC-2014-C1-015).

REFERENCES

Alkhalifah, T. and Choi, Y., 2012. Taming waveform inversion non-linearity through phase unwrapping of the model and objective functions. Geophys. J. Internat., 191: 1171-1178.

Aminzadeh, F., Burkhard, N., Nicoletis, L., Rocca, F. and Wyatt, K., 1994. SEG/EAEG 3-D modeling project: 2nd update. The Leading Edge, 13: 949-952.

Billette, F. and Lambaré, G., 1998. Velocity macro-model estimation from seismic reflection data by stereotomography. Geophys. J. Internat., 135: 671-690.

Brenders, A. and Pratt, R., 2007. Full waveform tomography for lithospheric imaging: Results from a blind test in a realistic crustal model. Geophys. J. Internat., 168: 133-151.

Brossier, R., Operto, S. and Virieux, J., 2010. Which data residual norm for robust elastic frequency-domain full waveform inversion? Geophysics, 75: R37.

Bunks, C., Saleck, F., Zaleski, S. and Chavent, G., 1995. Multiscale seismic waveform inversion. Geophysics, 60: 1457-1473.

Guitton, A., Symes, W., 2003. Robust inversion of seismic data using the Huber norm. Geophysics 68, 1310-1319.

Ha, T., Chung, W. and Shin, C., 2009. Waveform inversion using a back-propagation algorithm and a Huber function norm. Geophysics, 74: R15-R24.

Ha, W., Chung, W., Park, E. and Shin, C., 2012. 2-D acoustic Laplace-domain waveform inversion of marine field data. Geophys. J. Internat., 190: 421-428.

Ha, W. and Shin, C., 2012. Laplace-domain full-waveform inversion of seismic data lacking low-frequency information. Geophysics, 77: R199-R206.

Landa, E., Beydoun, W. and Tarantola, A., 1989. Reference velocity model estimation from prestack waveforms: Coherency optimization by simulated annealing. Geophysics, 54: 984-990.

Liu, Z. and Bleistein, N., 1995. Migration velocity analysis: Theory and an iterative algorithm. Geophysics, 60: 142-153.

Mora, P., 1987. Nonlinear two-dimensional elastic inversion of multioffset seismic data. Geophysics, 52: 1211-1228.

Pratt, R., Shin, C. and Hicks, G., 1998. Gauss-Newton and full Newton methods in frequency-space seismic waveform inversion. Geophys. J. Internat., 133: 341-362.

Pratt, R.G., 1999. Seismic waveform inversion in the frequency domain, Part 1: Theory and verification in a physical scale model. Geophysics, 64: 888-901.

Prieux, V., Lambaré, G., Operto, S. and Virieux, J., 2012. Building starting models for full waveform inversion from wide-aperture data by stereotomography. Geophys. Prosp., 61: 109-137.

Pyun, S., Son, W. and Shin, C., 2010. 3D acoustic waveform inversion in the Laplace domain using an iterative solver. Expanded Abstr., 80th Ann. Internat. SEG Mtg., Denver: 951-956.

Ravaut, C., Operto, S., Improta, L., Virieux, J., Herrero, A. and Dell'Aversana, P., 2004. Multiscale imaging of complex structures from multifold wide-aperture seismic data by frequency-domain full-waveform tomography: application to a thrust belt. Geophys. J. Internat., 159: 1032-1056.

Sen, M. and Stoffa, P., 1991. Nonlinear one-dimensional seismic waveform inversion using simulated annealing. Geophysics, 56: 1624-1638.

Shin, C. and Cha, Y.H., 2008. Waveform inversion in the Laplace domain. Geophys. J. Internat., 173: 922-931.

Shin, C. and Ha, W., 2008. A comparison between the behavior of objective functions for waveform inversion in the frequency and Laplace domains. Geophysics, 73: VE119-VE133.

Shin, C., Ha, W. and Kim, Y., 2013. Subsurface model estimation using Laplace-domain inversion methods. The Leading Edge, 32: 1094-1099.

Shin, C., Koo, N.-H., Cha, Y.H. and Park, K.-P., 2010. Sequentially ordered single-frequency 2-D acoustic waveform inversion in the Laplace-Fourier domain. Geophys. J. Internat., 181: 935-950.

Shin, J., Ha, W., Jun, H., Min, D.-J. and Shin, C., 2014. 3D Laplace-domain full waveform inversion using a single GPU card. Comput. Geosci., 67: 1-13.

Sirgue, L. and Pratt, R.G., 2004. Efficient waveform inversion and imaging: A strategy for selecting temporal frequencies. Geophysics, 69: 231-248.

Stoffa, P.L. and Sen, M.K., 1991. Nonlinear multiparameter optimization using genetic algorithms - Inversion of plane-wave seismograms. Geophysics, 56: 1794-1810.

Tarantola, A., 1984. Inversion of seismic-reflection data in the acoustic approximation. Geophysics, 49: 1259-1266.

Virieux, J. and Operto, S., 2009. An overview of full-waveform inversion in exploration geophysics. Geophysics, 74: WCC1-WCC26.

Warner, M. and Guasch, L., 2014. Adaptive waveform inversion - FWI without cycle skipping - Theory. Expanded Abstr., 76th EAGE Conf., Amsterdam: We E106 13.

White, D.J., 1989. Two-dimensional seismic refraction tomography. Geophys. J. Internat., 97: 223-245.

Wu, R.-S., Luo, J. and Wu, B., 2014. Seismic envelope inversion and modulation signal model. Geophysics, 79: WA13-WA24.